applied sciences

MDPI

Article

Electro-Thermal Properties of Carbon-Fiber-Reinforced Mortar Prisms

Jung-Young Son [1,*], Jung Kim [1], Tetiana Venkel [2], Jongun Park [1] and Gwanghee Heo [1]

[1] Public Safety Research Center, Konyang University, Nonsan 32992, Republic of Korea
[2] Linguistics for Sciences Department 26, 58012 Chernivtsi, Ukraine
* Correspondence: jyson@konyang.ac.kr; Tel.: +82-10-4232-5791

Abstract: The thermal properties of electrically heated carbon-fiber-reinforced mortar prisms with 0.5%, 1.0%, 1.5% and 2.0% of their volumes are investigated. Each prism dimension is 40 mm × 40 mm × 160 mm. When the constant power of 30W is applied to two conductive-gel strips painted on the prisms' surfaces as the electrodes, for 5 min, the prisms show that: (1) their surface heating patterns have mostly the shape of two semi-circles centered at each of the electrodes; (2) their surface temperatures increase more for those with higher fiber percentages; (3) their surface's average temperature increments are the highest for the first 1 min of heating; (4) the lines representing the lowest and highest temperature zones and one of the normal lines to two electrodes record the highest temperature increment for the first 1 min of heating; (5) the temperature ratio of two points on the surface of each of four different percentage prisms has almost an unchanging value for all heating time periods especially when the two points are close to the volume defined by two electrodes; (6) the average temperature increments decrease with time. These facts are for all percentage prisms.

Keywords: electro-thermal properties; fiber reinforced mortar prisms; resistance; conductive gel electrodes; heating with constant power

Citation: Son, J.-Y.; Kim, J.; Venkel, T.; Park, J.; Heo, G. Electro-Thermal Properties of Carbon-Fiber-Reinforced Mortar Prisms. *Appl. Sci.* **2023**, *13*, 3988. https://doi.org/10.3390/app13063988

Academic Editor: Ana Martins Amaro

Received: 14 February 2023
Revised: 17 March 2023
Accepted: 18 March 2023
Published: 21 March 2023

1. Introduction

The interest in developing conductive concrete increases with the growth of the number of traffic accidents incurred by black ice, which is known as the thin layer of ice on the surfaces of roads/airfield runways [1]. The conventional method of deicing roads is spraying various chloride products to roads/airfield runways [2]. It is effective but it damages cars/planes, roads, driveways and environments surrounding the roads/airfields in the long run. Hence, as an alternative method to the spraying, melting the ice by heating the road with electric power has been developed. However, the electric power can only be delivered by the electric current because it is linearly proportional to the square of the current. However, the concrete itself cannot flow electrical current because it is an electrical insulating material. To make the road able to flow the current, it should be made to have a certain electrical conductivity.

There are two known ways of making a road electrically conductive: one of them is embedded heat-generating electric wires underneath the surface, and the other is making the road itself to be a conductive material by mixing the concrete with materials that conduct electricity. However, since it has been known that the former is more costly and less reliable than the latter [3], more research has been done to develop conductive materials to be mixed with the concrete. Typical conductive materials are electrically conductive particles such as carbon black and steel powders, and carbon fibers (hereafter abbreviated as fibers in this paper) [4–7].

The conductive particles and the fibers differ in their mixability with the concrete. The particle form can be uniformly mixed with the concrete, but the fibers cannot. This is why the fibers are made to have a wire form and they are embedded into the concrete [6,7].

However, this is not a good method because it can reduce the physical strength of the concrete instead of reinforcing it. Nevertheless, since a certain amount of short fibers has often been mixed to reinforce the physical strength of the cement mortar due to their much higher tensile strength compared with the concrete [8–10], their electrical conductivity transforms the fiber-reinforced concrete into a conductive material. The electric conductivity of the fibers is in the range of 5×10^4~5×10^5 S (ampere/volt)/m (length) [11]. This conductivity value is much lower than that of metal. Hence, it can be used as a heat-generating electric wire, i.e., a heater that will generate enough heat to melt the ice and keep the road surface ice-free.

The conductivity of conductive concrete is estimated with embedded mesh-type wire grid electrodes placed at a fixed distance apart from each other. The resistance value between two electrodes is measured [12,13] because the conductivity is obtained by inverting the resistivity value, which is linearly proportional to the resistance value. The resistance is defined as the resistivity of the fiber/conductive particles multiplied by the distance between electrodes and divided by the electrode area. To heat the concrete, it is necessary to attach the electrodes to the concrete. Since the mesh-type embedded electrodes are just a wire grid formed by thin copper wires, each of these wires is localized, i.e., isolated by the surrounding cement/concrete in the concrete. Due to this isolation, the electric current will be confined within the area occupied by the wires. Since the area will be much smaller than that of the concrete cross-section holding the electrode, the resistance of the current will be very high. Hence, the large portion of the heat induced by the current will be dissipated near the electrodes. Therefore, heating the concrete by flowing current through the embedded wire grids will not be efficient.

It is possible to replace the wire grid with an electrically conductive glue. It can be painted on the surface of the concrete to be used as an electrode. This glue is highly convenient compared to the embedded wire grid electrode because an electrode of any shape can be formed on any location of the surface when it is needed. Moreover, the electrode can be printed on the rough surface of the concrete with good contact because the glue can smear into the surface due to its soft gel form. Hence, an electrode of any size can be doped on any road surface with the conductive glue.

In this paper, the electro-heating properties of mortar prisms reinforced with different amounts of fibers, particularly, 0.5%, 1.0%, 1.5% and 2.0% in the volume of sand mixed with cement are studied by analyzing heat distribution patterns on their surfaces. The prisms' surfaces are painted with a conductive gel to be used as electrodes. Three mortar prisms for each fiber percentage are used.

2. Experimental Samples and Experimental Set-Up

Three mortar prisms reinforced with each of the four volume percentages of fibers, namely, 0.5%, 1.0%, 1.5% and 2.0%, are prepared according to the Korean Standard [14]. The fibers are bundled to have a diameter of 7 ± 2 μm and then cut into 6 mm in length before being added to the mortar mixture. The preparation details of the fiber to mix with the mortar are described in [15]. The prism dimensions are 40 mm × 40 mm × 160 mm and their designed weight is 500 g [15]. They were kept in a water reservoir for 28 days for curing. Three samples for each fiber percentage were prepared. Each of these prisms was broken into two parts due to the flexural strength test undertaken [16]. Thus, six pieces for each fiber percentage were obtained. These pieces are not of same size because each sample is broken into two pieces by the crack induced by the test.

Hence, the length of each piece is either slightly longer or shorter than 80 mm, i.e., a half of the prism's length of 160 mm. These broken sample pieces had been kept in laboratory condition for almost three years. They were expected to be nearly dried because the plane mortar prisms that were stored together with the samples revealed that their resistances far exceed the Fluke's handheld multimeter's measuring range and their weights do not have the designed value. All of them have lower values than the designed value due to the presence of fibers.

Table 1 shows the sample weight measured with a precision scale (Cas: cas-USA.com). It includes the weight of plane prisms. The weights of two broken left and right pieces of each sample and the sum and average of the same percentage prisms are also shown. The table shows that the same percentage prisms have almost the same weight, though between different percentage prisms, the weight differences are prominent. Only 1.0% prisms are near 500 g while other percentage samples are much lighter than the 1.0%. The average weight of the 1.0% prisms is 499 g. The weight is reduced to 495 g, 467 g, 462 g and 432 g for the 0.5%, 1.5%, 0.0% and 2.0% prisms, respectively. When the average weights of other percentage prisms are normalized by that of the 1.0% prisms, the values are given as 0.99, 0.94, 1.0, 0.93 and 0.87 for 0.0%, 0.5%, 1.0% 1.5% and 2.0%, respectively.

Table 1. Weights of four different percentage prisms: Each percentage has 3 prism samples.

	Sam. No.	Left (g)	Right (g)	Sum (g)	Weight (g) (Average (g))
0.0%	1	216	248	464	1386 (462) *0.93
	2	232	230	462	
	3	225	235	460	
0.5%	1	246	250	496	1486 (495) *0.99
	2	248	247	495	
	3	273	222	495	
1.0%	1	203	294	497	1497 (499) *1.0
	2	241	259	500	
	3	241	259	500	
1.5%	1	247	222	469	1400 (467) *0.94
	2	227	235	462	
	3	245	224	469	
2.0%	1	195	241	436	1296 (432) *0.87
	2	204	222	426	
	3	212	222	434	

These values are also specified in Table 1. The 2.0% prism reveals the smallest value. The highest weight recorded by 1.0% prism implicitly informs that the number of air pockets in the prisms is the smallest. The number of air pockets decreases as the fiber percentage increases [15]. This is why the weight of the plane prism is slightly greater than that of the 2.0% prism. The increasing fiber percentage reduces the prism's weight, but the decreasing rate in the number of the air pockets is greater than the weight reduction rate due to the growth of the fibers volume. The weight of the plane prisms allows estimating the density of the plane prisms. It is calculated as 1804.69 kg/m^3. This density value is almost the same as that of the fiber (Toray (Japan)'s intermediate modulus type T1100G), which is specified as 1800 kg/m^3. The density value of the plane prisms also implicitly indicates that they lost most of their moisture.

To heat the prisms, the DC (Direct Current) power supply should be able to regulate current up to 5 A and voltage to 30 V for electrical heating. For electrical heating, a conductive gel is painted on one surface of each piece and its opposite side along the bisecting line of the piece in its length direction in order to have the shape of a rectangle with dimensions of 40 mm $\times$ 5 mm. The rectangle shape is selected to observe the heat diffusion to its two sides. Figure 1 shows the electrode preparation in each prism piece; the electrode connection is also shown. A conductive gel electrode with a thickness of 5 mm is drawn on one surface of each piece. On the opposite surface of the piece, another electrode with the same dimension and direction as the first one is drawn. The electrode is located near the middle area of each piece. One of the electrodes is connected to the '+' terminal of the power supply and the other to the '–' terminal or ground terminal through electric wires. These wires are in contact parallel to the long side directions of their corresponding electrodes. The typical resistivity of the conductive glue is around 0.09 Ω·cm to 0.0001

Ω·cm [17]. The resistivity can go up several tens percent more when it is heated [17], but it is still very small compared with that of the dried prisms/concrete, which is in the range of 100 Ω·cm to 1,000,000 Ω·cm [18].

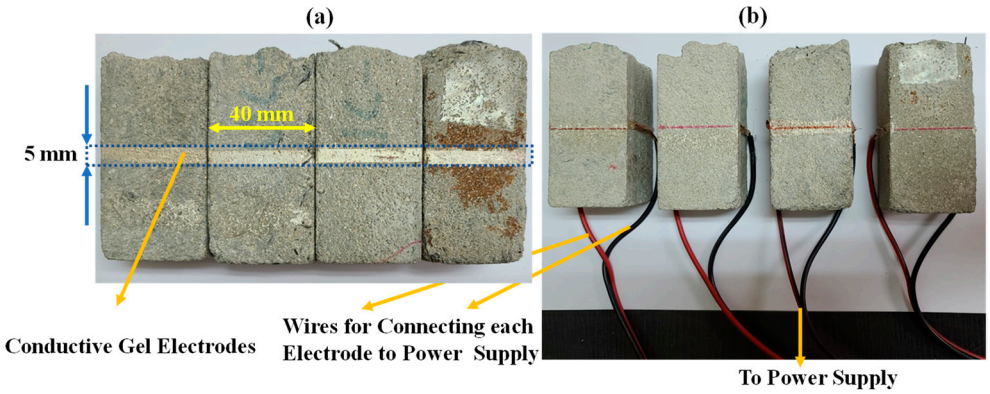

Figure 1. Conductive gel electrode and wire-connection preparation on the prisms. (**a**) Conductive gel electrode. (**b**) Wire-connection preparation on the prisms.

These rectangles are working as electrodes. However, the contact between these electrodes and the fibers in the prism piece can be hardly achieved due to mortars covering the fibers. This ill connection problem is worsened when the densities of fibers under the electrodes become lower. This ill connection and fiber density may be the decisive factors of determining the resistance values of different fibers percentage prisms and different prisms of the same fiber percentage. Hence, it is expected that the resistance values of the prisms will be reduced as the fiber percentage increases. This resistance decrease also reduces the resistance introduced by the ill connection, but it will still take the highest portion of the resistance in the higher fiber percentage prisms.

It is also considered that the contact between electrodes and wires can also contribute some resistance because the wires cannot be fully in contact with the electrodes. The electrodes do not have a smooth surface because they are drawn on the prisms' rough surfaces. It is shown in the experiments that the resistance induced by the ill connection, lower density and unsmooth electrode surfaces is much larger than that of the fibers in the different percentage prisms. Since the resistance will induce heating near the surface of the prisms, a certain amount of electric power can be ineffectively consumed. To minimize this inefficient consumption of power, it is necessary to tighten the electric wires to the electrodes as much as possible.

Figure 2 shows the experimental set-up. The set-up consists of a power supply for applying both voltage and current to the prism to be heated, a multimeter for measuring the resistance of the prism before applying power to determine the necessary current and voltage values for applying 30 W power, a bench vise for connecting the electric wires tightly to the gel electrodes, a thermal camera for photographing the thermal image, i.e., the prism's surface temperature variation with time, and a notebook for recording the thermal images as files. The prism's surface in the thermal image is one of the prism surfaces between the electrode surfaces. The thermal camera is fixed directly above the prism at a distance of 500 mm.

Through the wires, 30 W of power was applied to each prism for up to five minutes. Therefore, the total energy deposited to each prism is 9 KJ (30 W × 60 sec × 5 Min.). FLIR T640 thermal camera, which has a pixel resolution of 640 × 480, a pixel size of 17 μm and temperature resolution of 0.03° K at 30 °C, was used to determine the surface temperature distribution of the prism, before applying the power and every thirty seconds of heating. The thermal image from this camera can show the heating level of the test objects with a temperature distribution represented by a different color combination.

Figure 2. Experimental set-up.

When the voltage is applied to the prism through the electrodes, the current induced by the voltage takes the path that reveals the lowest resistance. Hence, the ideal prism volume that will provide the paths to the current are calculated as 40 mm × 40 mm × 5 mm = 8000 mm^3, as shown in Figure 3, because the resistance is linearly proportional to the path length. The path should be as short as possible while it is considered that the prism has a uniform resistance. The shortest path of connecting two electrodes is just the straight line normal to the electrodes. The prism volume defined by the shortest path represents the minimum volume that will be heated in any circumstance when the voltage is applied to the electrodes. This volume will have the maximum weight of 15.63 g (500 g × 5 mm/160 mm).

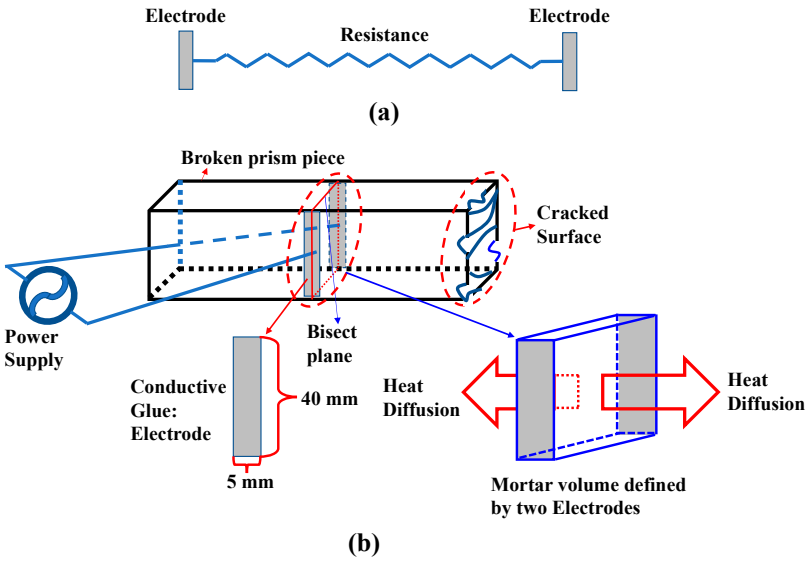

Figure 3. Equivalent circuit of the mortar prisms. (**a**) Equivalent circuit of the prisms. (**b**) A schematic of electrical connection.

Figure 3 shows an equivalent electrical circuit of the prisms (Figure 3a) and electrical connection diagram of the experimental set-up (Figure 3b). The equivalent circuit can be represented as the two electrodes and the resistance represents the total resistance of the volume. In practice, the volume that provides the current path will always exceed the minimum volume because the fibers, which are the main current path in the prism, are randomly directed, aligned and distributed in the form of a strand, strands, bunches and balls [15,19]. This means that there may not be any uniformly connected path between

the electrodes and, hence, the lowest resistance path may not always be the straight line normal to the electrodes. The path is defined by the size and amount of the clustered fiber strands and their aligned and connected directions. In each position of this path, the fibers are differently heated by the current because of the resistance differences for various positions. The path has a non-uniform heat distribution. Therefore, the minimum volume is hardly identified. The path works as the heat source because the electric power is deposited to the path. The heat from the path radiate, convect to the surrounding space and diffuse to its neighboring volumes. By diffusion, the entire prism is heated. This is why the temperature distribution along the length direction of the prism may reveal the heat diffusion/distribution pattern.

3. Some Relationships Governing the Mortar Prism Heating with the Electric Power

When a voltage $V$is applied to two electrodes attached to a material with resistance R, then current I, flowing through the channel between the electrodes, and power P, deposited on the material, are expressed as [20]:

$$I = V/R \tag{1}$$

$$P = VI = RI^2 = V^2/R \tag{2}$$

Equations (1) and (2) indicate that the power deposited on the material is inversely proportional to the resistance. This means that the power applied to the material with higher resistance will be smaller for a given voltage. Power P has the unit of W(Watt), while V and I values have the units of volt (V) and ampere (A), respectively. Resistance R has the unit of Ω (Ohm) and is related with resistivity ρ as,$R = \rho A/l$, where A (mm^2) is the average of the two electrode areas and l(mm)is the thickness of the material. Energy E deposited on the material by the given power P is described as $E = Pt$ J(Joule), where t is the time of applying power to the material in seconds.

Due to this energy, the temperature of the material will increase. The temperature increments ΔT, due to the deposited electric power, Pt, is expressed as [21]:

$$\Delta T = E/mS \tag{3}$$

where m denotes mass of the minimum volume, as shown in Figure 2, in the unit of Kg, and S is specific heat of the material in the unit of J/(Kg·K), where K is the absolute temperature. For the specific heat of the mortar prism, 980 J/(Kg·K) is used [22]. Since the temperature increment is inversely proportional to the prism weight as shown in Equation (3), the smaller weight prisms will gain higher temperatures. This should be normalized by considering their weights to correctly compare the thermal properties of the prisms with different fiber percentages.

The normalized numbers calculated previously, which are specified with an asterisk (*) in Table 1, work as the compensation factor for each percentage prisms. When the factor is multiplied by its corresponding temperature increment, the increment should be the same as that of the 1.0% prisms. However, since the presence of fibers with different volume percentages transforms the prisms with different fiber amounts to the materials with different conductivities, the actual temperature increment will be different for different fiber percentages. The compensation factor should be multiplied by the temperature increments from the heating.

4. Experimental Results

Before electrical heating, the resistances of the prisms were measured with a digital multimeter [23]. However, for the plane prisms, no heating was deposited to them because of their very high resistances. Since the plane prisms do not include any conductive material, their resistances cannot be measured with the multimeter. The resistance values of the fiber-reinforced prisms are summarized in Table 2. The resistance values of the

front–back and top–bottom sides of the minimum volume specified in Figure 2 for three prisms of each fiber percentage are shown in Table 2. This table also presents the averaged resistance values of all three prisms specified as 1, 2 and 3, and the front–back and top–bottom sides specified by "a" and "b", respectively. In addition to the abovementioned values, the dynamic resistances of the different fiber percentage prisms under heating are also shown with the applied voltage, current and power.

Table 2. Measured and calculated resistances of prisms of 4 different percentages.

Sample	1		2		3		Total Average (Ω)	Applied Power(W) (Voltage(V), Current(A))	Dynamic Resistance(Ω) (Temp. Incre.)
Side	a (Ω)	b (Ω)	a (Ω)	b (Ω)	a (Ω)	b (Ω)			
Prism	Average (Ω)		Average (Ω)		Average (Ω)				
0.5%(Ω)	16.7	28	24	24	12	22	21.12	30.25 (26.3, 1.15)	22.87 (119.71)
	22.35		24		17				
1.0%(Ω)	8.3	7.5	6	6.8	5.1	8.5	7.0	29.92 (13.6, 2.2)	6.18 (117.24)
	7.9		6.4		6.8				
1.5%(Ω)	5.4	4.9	6.5	4.8	5.2	5.0	5.3	30.0 (12.5, 2.4)	5.21 (127.22)
	5.15		5.65		5.1				
2.0%(Ω)	5.1	4.2	4.4	4.8	3.7	4.3	4.42	29.97 (8.1, 3.7)	2.19 (137.83)
	4.65		4.6		4.0				

Table 2 informs about the following:

(1) The average resistance value of the same fiber percentage indicates that, as the fiber percentage increases, the resistance values decrease; the values are 21.1 Ω, 7.0 Ω, 5.3 Ω and 4.4 Ω, for the 0.5%, 1.0%, 1.5% and 2.0% prisms, respectively;
(2) The resistance values of "a" and "b" are not the same and the three prisms of the same fiber percentage numbered 1, 2 and 3 have slightly different resistance values even if they were made from the same batch mortar mix;
(3) The difference between the lowest and the highest resistance values is 16 Ω, 2.5 Ω, 1.7 Ω and 1.4 Ω for the 0.5%, 1.0%, 1.5% and 2.0% prisms, respectively.

However, the actual resistance values calculated from the voltage and current values (voltage/current) are 22.9 Ω, 6.2 Ω, 5.2 Ω and 2.2 Ω for the 0.5%, 1.0%, 1.5% and 2.0% prisms, respectively. These values are nearly the same as their corresponding average values, except for the 2.0% prisms.

Item (1) confirms that the conductivity of the prisms is originated by the fibers. Otherwise, the fiber percentage increase does not induce the further increase in the conductivity values, i.e., decrease in the resistance values. In addition to this, Equations (1) and (2) inform that more power will be applied to the prism as the fiber percentage increases. Item (2) indicates that the fibers in the prisms are not uniformly distributed because the conductivities of the mortar prisms are brought by the fibers. As indicated in Item (3), the reducing resistance difference between prisms of the same fiber percentage tells that the fibers become more uniformly distributed in the prisms as the fiber percentage increases.

Item (3) also shows that the actual resistances for the 0.5%, 1.0% and 1.5% prisms are slightly different from their corresponding average values, but for the 2.0% prism, the value is half of the measured resistance value. The reason is not completely clear, but it could be caused by the loosely contacted fibers, which become tightly connected to each other by the heat induced by the current flowing through the fiber. As shown in Equations (1) and (2), the resistance decrease will cause applying more power to the prism. This power increase will induce further increase in the temperature of the prism. This increase squeezes the fibers in the prism more due to the growing thermal expansion of the prism. The fibers squeezing will improve the connection between fibers, which, in turn, will cause the decrease of the resistance. The resistance decreases in the 2.0% prism when the power is applied will be the result of the improvement.

Figure 4 shows the full frame thermal image of a piece of a 1.0% prism to specify the surface area for determining the average temperature and the lines to show the heat diffusion/temperature distribution patterns of the different percentage prisms. The total resolution of the image is 640 × 480, but the surface area of the piece is approximately 444 × 222 pixels. The trace of the discarded conductive gel electrode is also shown in the middle of the prism. The vertically aligned rectangle in this trace represents the location of the minimum volume defined by the 5 mm width electrodes. Since the 222 pixels correspond to 40 mm, the width of the rectangle corresponds to 28 (~222 × 5/40) pixels.

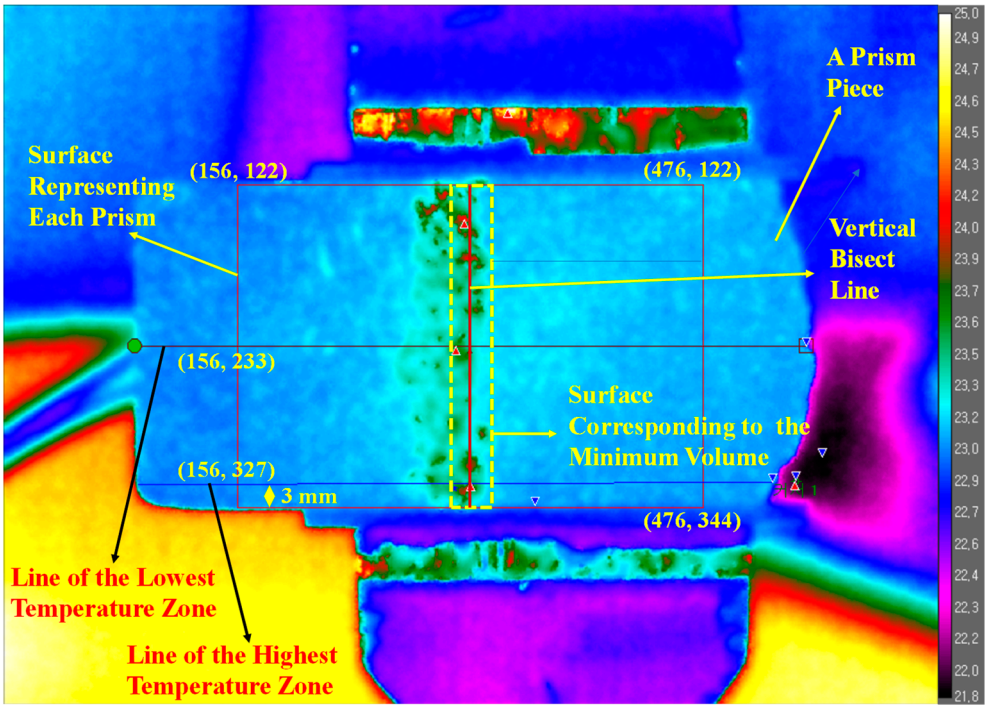

Figure 4. Position of lines and surfaces for measuring temperature increments. The temperature distribution is less than 25°. The prism surface is in the 23° range.

When there is no heat diffusion, the electric power will heat the volume, which works as the heat source defined above. Thus, the expected temperature increments predicted by Equation (3) will be 119.71°, 117.24°, 127.22° and 137.83° for the 0.5%, 1.0%, 1.5% and 2.0% prisms, respectively, when the weight and the applied electric power differences of each percentage prism from other prisms as shown in Tables 1 and 2 are considered. However, in practice, the temperature increase will be much lower than the value given above due to the fact that (1) the heat source has higher volume than the minimum one, (2) the heated volume will radiate the heat to the surrounding space through radiation and convection, and (3) some heat from the volume will be diffused to the neighbors. Due to this diffusion and the electrical paths formed outside of the volume, the temperatures of the volume surrounding the minimum volume will also increase.

As the prism temperature increases, the prism's overall resistance can decrease. The increasing temperature will induce the prism to expand. The expansion of the prism will cause stronger squeezing of the fibers in it. This squeezing will force the fibers to contact/connect themselves more tightly. This tightened contact/connection will reduce overall resistance of the prism, which will be reduced even further as the fiber amount increases. This could be the reason why the heated state resistance of the 2.0% prism is reduced to a half of its unheated state resistance. However, this decreased resistance could revert to its unheated value when the prism is cooled.

Since the presence of the minimum volume is hardly identified due to thermal diffusion, the accurate estimation of the electric power deposited to the volume will not

be possible. For estimation, the average temperature of the surface area defined by the rectangle with 320 pixels in horizontal and 222 pixels in vertical direction are found. These pixels correspond to 57.66 mm × 40 mm of the surface area. This rectangle is specified by the four corner pixels having the positions of (156, 122), (476, 122), (156, 344) and (476, 344), as shown in Figure 4. It is expected that the 57.66 mm dimension covers most of the prism lengths because the prism pieces are not of the same size, and their broken faces have very bumpy profiles.

Along with the averaged surface temperature, observed are the temperature distributions of the horizontal line that bisects the prism piece into two horizontal parts and another horizontal line at 3 mm distance from the bottom edge of the piece. The former represents the lowest temperature and the latter represents the highest temperature zone of the heated prism. The bisecting horizontal line will pass the pixels (156, 233) and (156, 327), and the other line will pass the pixels at (156, 233) and (156, 327) in Figure 4. These temperature distributions are used to show the heat diffusion pattern of the prism. The relative positions of the lines and sizes of the rectangles in other percentage prisms are also the same.

Apart from these lines and rectangle, the average temperatures of the broken rectangle in the middle part of the piece, which corresponds to the surface areas of the minimum volume, and the vertical bisect line of this rectangle are also found to identify the heat deposition pattern with time. In fact, the vertical bisect line represents the line connecting the centers of two electrodes, where the wires from the power supply are in contact. This line will be one of the normal lines to two electrodes.

In Figure 5, the thermal images of the electrical heating for the 0.5%, 1.0%, 1.5% and 2.0% prism pieces are shown. These images show the temperature distribution pattern for the heating time specified at each image. However, it is expected that this distribution pattern may not be the same as those of different cross-sections of the volume underneath the surface because of inhomogeneity of the prisms. The temperature range of each thermal image is normalized from 22.8° to 80° to compare the temperature variations of different percentage prisms with heating time. The color bar on the right side of the images informs about the temperature corresponding to each color. The numbers in the bar represent the temperature of each color. The dotted rectangle in each image represents the surface area corresponding to the minimum volume. When a voltage is applied through the electrodes, a current loop is formed by the wires connected to the "+" terminal of the power supply, electrode, fibers in the minimum volume, opposite side electrode and wires connected to the "−"/ground terminal of the power supply. In this loop, the overall resistance is the sum of the resistances from the contacting parts of (1) the wires and the electrodes, (2) the electrodes and fibers in the volume, and (3) the fibers themselves. Among these three, the highest resistance will be that from the contacting part of the electrodes and fibers. Due to this resistance, the heat contribution from the fiber heating will not be significant.

The temperature distribution pattern indicates that the heat is mostly generated at the surface of the piece, where the wires, the electrodes and the fibers near the electrodes meet. The applied electric power is mostly deposited at the interfaces between the electrodes and the fibers. That is why the heat distribution pattern has the shape of a half circle. The heat from the interfaces is diffused radially to the inside of the prisms. However, since the interfaces are not completely parallel to the electrode's long sides and they are different for different electrodes, the two circles do not have the same radius and they are somewhat distorted. As shown in the 240 sec images, the radii of the circles increase as the fiber percentage increases, though the difference between 0.5% and 1.0% is not prominent. This means that the prisms with higher fiber percentage will be heated more.

The amount of the diffused heat reduces as the radius of the circle increases and the area between these two half circles, i.e., the middle part of the prism is heated less due to its smaller resistance compared with the near-electrode parts. This makes the temperature of the middle part much lower than the electrode side. However, as the heating time increases, a clearly visible heated corridor having a width comparable to the dotted rectangle in each

image appears between these two circles, as shown in the 270 sec image of 0.5%, 240 sec images of both 1.0% and 1.5%, and 180 sec image of 2.0%. These corridors identify the presence of the minimum volume. The further increase in the heating time induces the circles to contact and overlap with each other, as shown in the 300 sec image of 1.5% and the 240 sec and 300 sec images of 2.0%. Figure 5 also shows that the circles have bigger radii as the fiber percentage increases.

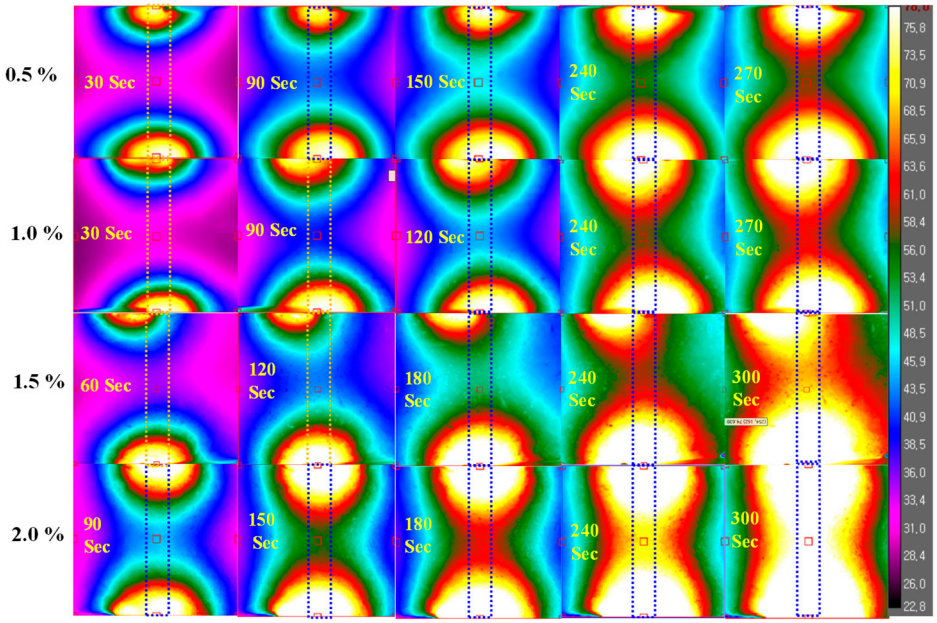

Figure 5. Heat/Temperature distribution patterns of a prism set. The dotted vertical rectangle and the time in each temperature distribution represent the surface area of the minimum volume and the heating time, respectively.

Figure 6 shows thermal images for different pieces of the percentage prisms, different from Figure 5.

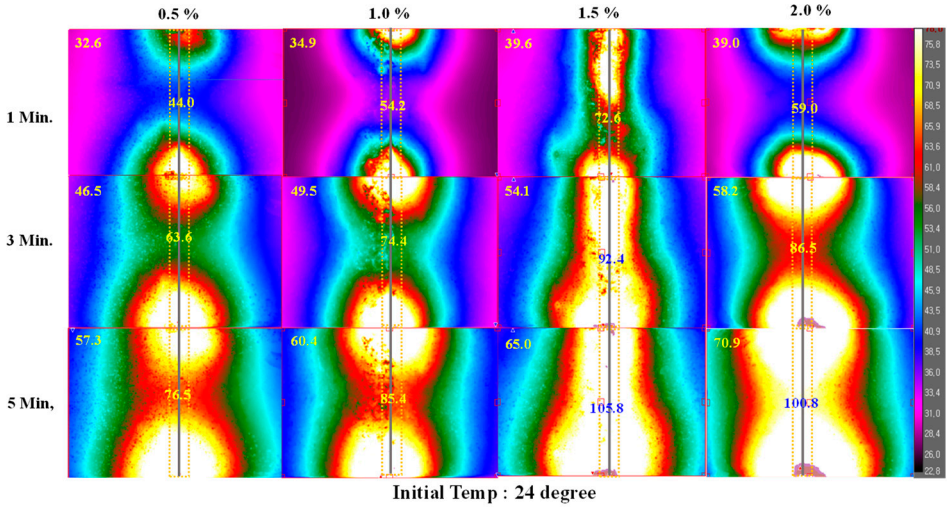

Figure 6. Heat/Temperature distribution patterns of another prism set. The numbers represent average temperatures of the prism surface (**top left** corner of each image) and the minimum volume surface (**middle**). The dotted vertical rectangle and the solid line in each temperature distribution represent the surface area of the minimum volume and the bisect line of the rectangle, respectively.

Only three thermal images at 1, 3 and 5 min of heating for each percentage prism are combined to show the temperature distribution changes in the prism surface with the

heating time. The dotted rectangle in each image represents the surface area corresponding to the minimum volume. Each image corresponds to the surface area of 57.66 mm × 40 mm specified in Figure 4. The numbers in the left corner and the center of each image indicate the average temperatures of the surface area and the dotted rectangle, respectively, during the initial temperature, i.e., the temperature before heating, which is 24°. Thus, the actual temperature increment by the electric power will be the numbers minus 24°, i.e., 8.6° (32.6–24°) for the 1 min case of the 0.5% prism in Figure 6.

The temperature range of each thermal image is normalized from 22.8° to 80° for comparison. The color bar is the same as in Figure 5. The color changes from black, purple, blue, green, red and yellow to white, corresponding to the lowest to the highest temperature. Therefore, as the time increases, more surface areas of each prism turn red, yellow and white. The temperature distribution patterns are very similar to the images in Figure 5, except for the 1.5% prism. For the 1.5% prism, the bottom electrode pattern is the same as the 1.5% patterns in Figure 5, but the top electrode pattern has a cucumber shape that almost fits inside of the rectangle. This identifies the presence of the minimum volume and indicates that the resistance value of the minimum volume under the cucumber-shaped area is almost the same as that of the interface between the electrode and fibers. This part of the minimum volume is almost equally heated by the electric power.

The images for the 3 and 5 min durations show that the top and bottom patterns overlap each other and extend outside the rectangle. Figure 6 reveals the following:

(1) The waveforms of the temperature distributions are somewhat smoothly varying with their peaks near the left and right edges, and their minimum is at their middle parts. However, for the 1.5% prism, the smoothness is greatly reduced and their right peaks are away from the edge. This is probably caused by its unique heating pattern.
(2) The recorded average temperature (the temperature increment from Equation (3) of the minimum volume for 1 min heating is 20.0° (119.71°), 30.2° (117.24°), 48.6° (127.22°) and 35.0° (137.83°) for the 0.5%, 1.0%, 1.5% and 2.0% prism, respectively. The calculated temperature increment is in the order of 2.0%, 1.5%, 0.5% and 1.0% because the weights of the prisms increase with the opposite order of the increment, as shown in Table 2. The recorded average temperature is much smaller than expected. This considerable difference could be caused by (a) the heat diffusion and (b) the current paths outside of the minimum volume.
(3) The average temperature is higher in the order of 0.5%, 1.0%, 2.0% and 1.5% prism for all heating time periods.
(4) The temperature increment for 1 min is 20° (0.5%) to 48.6° (1.5%); 19.4° (0.5%) to 27.5° (2.0%) for 1 to 3 min, and from 11° (1.0%) to 14.3° (2.0%) for 3 to 5 min. The greatest temperature increments are recorded within 1 min, and the increment decreases as the heating time grows.

Table 3 shows the increments of the surfaces' average temperature specified in Figure 6. The 'Incre' in Table 3 is the temperature increment from the previous heating time. This table reveals that there are no distinctions described in items (3) and (4) for the minimum volume. The average temperature of the surface area informs the following:

(1) The temperature increments are 8.6°, 10.9°, 15.6° and 15.0° for the 0.5%, 1.0%, 1.5% and 2.0% prisms, respectively, for the first 1 min of heating; this shows that the temperature increases more for higher fiber percentage prisms, though the temperature of the 1.5% prism is slightly higher than that of the 2.0% prism.
(2) The temperature increments for the first 1 min are higher than those for 1 to 3 min for both the 0.5% and 1.0% prisms, and they are almost the same for the 1.5% and 2.0% prisms.
(3) For the 3 to 5 min cases, the increments for 0.5% and 1.0% are slightly different from the first 1 min, but for the 1.5% and 2.0% prisms, the increments are smaller than those for the 1 min and the 1 to 3 min cases.
(4) The prism volume covered by the surface is about 11.43 times of the minimum volume. This indicates that the average temperature increments for 1 min heating cannot

exceed 10.47°, 10.26°, 11.13° and 12.06° for the 0.5%, 1.0%, 1.5% and 2.0% prisms, respectively, but these temperature values are smaller than the measured values described in item (1), except for the 0.5% prism. This informs that the volumes underneath the surfaces of the 1.0%, 1.5% and 2.0% prisms have much lower temperature increments than their corresponding surfaces.

(5) For the 3(5) min heating cases, the temperature increments expected from Equation (3) are 31.41° (52.35°), 30.84° (51.30°), 33.48° (55.80°) and 36.51° (60.85°) for the 0.5%, 1.0%, 1.5% and 2.0% prisms, respectively. However, the average temperatures of the surfaces shown in Figure 6 are 22.5° (35.2°), 25.4° (36.4°), 30.1° (41.0°) and 34.2° (46.9°), which are smaller than those from Equation (3) for all percentage prisms. The ratios of these measured and those from Equation (3), i.e., the heating efficiencies are 0.72 (0.67), 0.82 (0.71), 0.9 (0.74) and 0.94 (0.77), respectively. The ratios are higher for the higher percentage prisms, and they are decreasing with time. Furthermore, the differences between different percentage prisms are reducing. The ratio differences between the 0.5% and 2.0% prisms are 0.221 (0.1). This may mean that the temperature distribution patterns of the volumes underneath the surfaces become more uniform and similar to those of their corresponding percentage prisms. In any case, the temperatures indicate that the average temperature increments of the surfaces are the highest for the case of 1 to 3 min heating. However, the time period is 2 times that of the first 1 min case. When this time length is considered, the first 1 min heating induces the highest temperature increment for all the prisms.

(6) The average temperature of the 2.0% prism is higher than that of the 1.5% for 3 min heating. This is probably caused by the light weight of the 2.0% prism compared with the 1.5% one and the resistance decrease in 2.0% prism as explained before.

Table 3. Prisms' temperature increments for three different heating time periods of the first 1 min, 1 to 3 min and 3 to 5 min.

Prisms	Temperature Increment						Remark
	Incre.	1 min	Incre.	3 min	Incre.	5 min	
0.5%	8.6°	8.6°	13.9	22.5	10.8	33.3	Incre.: Increment -> Temperature increment between heating periods
1.0%	10.9	10.9	14.6	25.5	10.9	36.4	
1.5%	15.6	15.6	14.5	30.1	11.5	41.6	
2.0%	15.0	15.0	21.2	36.2	10.7	46.9	

Figure 7 shows the temperature distributions along the vertical bisect lines of the dotted rectangles in Figure 6. The distribution pattern has a non-uniform shape because of the non-uniform distribution of fibers with different resistances along the line. The numbers in these distributions represent the average temperature of the distributions. However, since the default value of the maximum temperature recorded is 160.2°, the top parts of the waveforms for the 2.0% prism are missed for the 3- and 5-minute heating.

It is also noticed that the average temperature values of the 1.5% prisms are higher than those of the 2.0%, but the peak intensity values are opposite. This informs that the temperature, i.e., the heat in the 1.5% prisms is more distributed than that in the 2.0% prisms. Figure 7 shows that the waveforms of the distributions at 1, 3 and 5 minutes heating for each percentage prism are of almost the same shape. This means that the temperature ratio of one point $\underline{a}$ to another point $\underline{b}$ on each of these lines is a fixed value for a prism.

The average temperature increment is within 20.2° (0.5%) to 50.8° (1.5%) for first 1 min, 19.5° (0.5%) to 26.9° (1.5%) for 1 to 3 min, and 10.3° (1.0%) to 13.9° (2.0%) for 3 to 5 min. The temperature increment is the highest for the first 1 min of heating and then reduces as the heating time increases. In fact, the temperature increment for the first 1 min is much higher than those for 1 to 3 min and 3 to 5 min. These increment characteristics closely match

those of the broken rectangles specified in Figure 6. However, the average temperature of the surface does not follow this increment pattern.

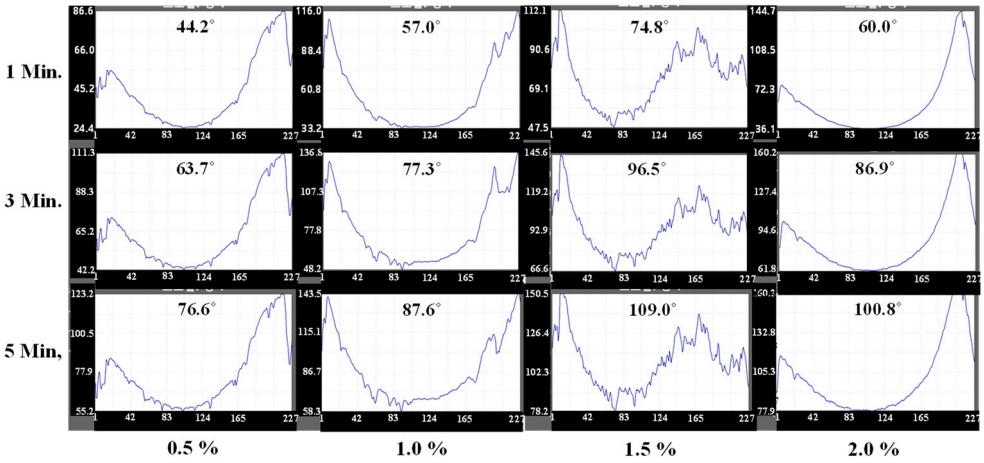

Figure 7. The waveforms of temperature distribution patterns along the vertical bisect lines: The vertical and horizontal axes represent temperature and pixel numbers from top to bottom of the vertical bisect line, respectively.

Figures 8 and 9 show the temperature distributions of the horizontal line at 3 mm distance from the bottom edge of the piece and the horizontal line bisecting the prism piece into two horizontal parts, respectively, for the 0.5%, 1.0%, 1.5% and 2.0% prisms. They show that the temperature distributions of the horizontal bisecting line are smoother than that of the 3mm distance horizontal line, though the 1.5% case does not show much difference between them. This may be caused by its unique heating pattern, shown in Figure 6.

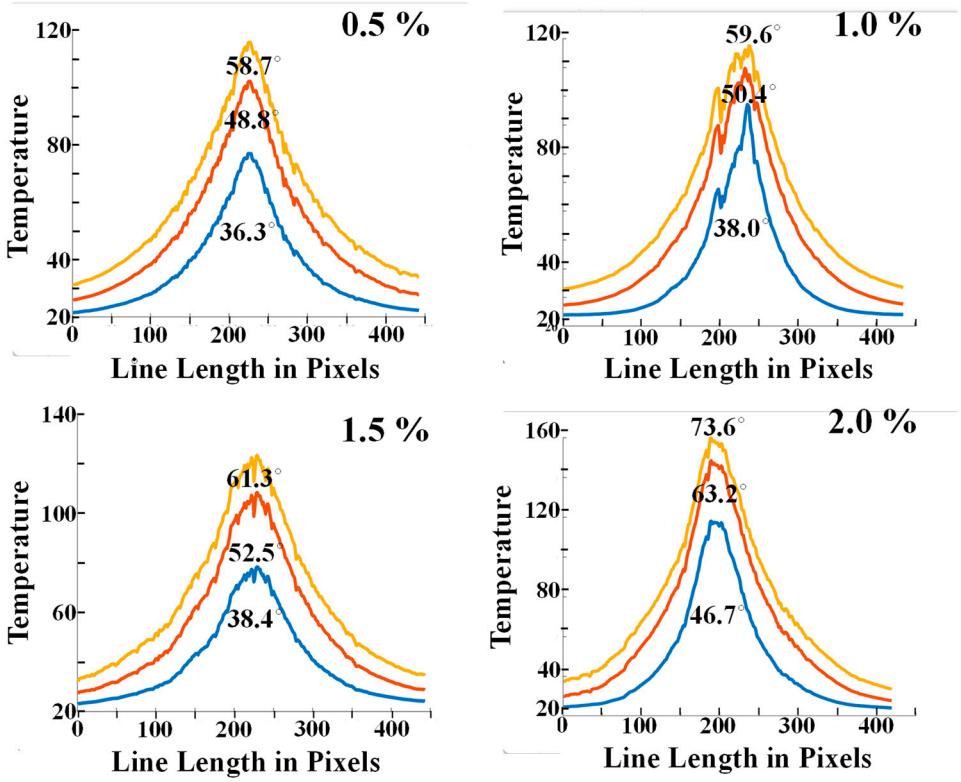

Figure 8. The temperature distribution pattern of along the line representing the highest temperature zone. The number in each curve represents the average temperature of the area covered by it.

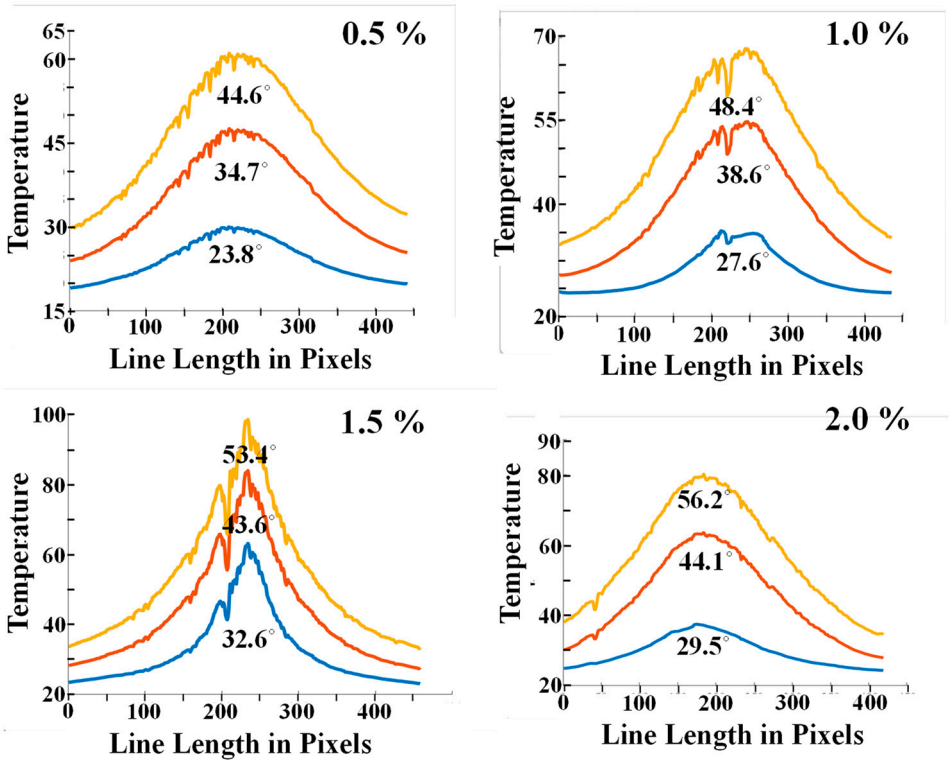

Figure 9. The temperature distribution pattern of along the line representing the lowest temperature multizone. The number in each curve represents the average temperature of the area covered by it.

For each fiber percentage, three distributions for 1, 3 and 5 min heating from bottom to top are shown. The average temperatures are specified on each of the distributions. The three distributions of each percentage prism have a similar waveform if they are drawn to have the same scale, as shown in Figure 7. The similarity increases closer to the middle part of the waveforms. In fact, they look almost the same at their middle parts. However, the similarity decreases closer to both edges of the waveforms. This is especially noticed in the waveforms of the 1 min heating. This can be explained if it is considered that the heat diffused to the sides does not have enough energy to meaningfully increase the temperatures of the edge sides. In fact, the temperature of these sides is lower than the initial average temperature 24° of the 1 min heating case.

These waveform characteristics are not different from those of the vertical line in Figure 7. It means that the temperature ratio of a point *a* to another point *b* on each of these prisms has a fixed value. This value will be more valid as the points are nearer to or within the minimum volume. The average temperature values are higher for the higher fiber percentage prisms for all heating time periods in both Figures 8 and 9, except for 1 min heating of the 1.5% and 2.0% prisms in Figure 9. This difference may be the result of the unique heating pattern of the 1.5% prisms.

The differences between the average temperatures of the 3 mm distance and the bisecting lines for the three heating periods are in the range of 12.5° to 14.1° for the 0.5%, 10.4° to 11.8° for the 1.0%, 5.8° to 8.9° for the 1.5%, and 17.2° to 19.1° for the 2.0% prism. These temperature ranges do not overlap each other; the smallest temperature difference is observed in the 1.5% prism and the highest in the 2.0% prism. This indicates that the 1.5% prism is heated more uniformly than other prisms, and the 2.0% has the worst uniformity among the four percentage prisms. The maximum difference between the lowest and the highest temperatures in the ranges, 3.1° (8.9–5.8°), indicates that the average temperature differences between the two lines, i.e., between the highest and the lowest temperature distributions in each percentage prism are kept nearly the same without regarding the heating time periods.

Figure 10 presents graphical comparison of the variation in the average temperature increment of the surface with the heating time for four percentage prisms. The temperature values in this graph are obtained by averaging the temperature increments of the prisms shown in Figures 5 and 6 (Figure 10a). Since there are some differences between prism weights and the electric power applied to the prisms, these differences should be compensated for accurate comparison. For this purpose, the weight is normalized in the way that is described in Section 2, while the electric power shown in Table 2 and the weight are the same as for 30 W. The compensation factors are calculated as 0.982 for the 0.5%, 1.0 for the 1.0%, 0.924 for the 1.5%, and 0.853 for the 2.0% prism. Figure 10a is compensated by these normalization factors as shown in Figure 10b. Figure 10a shows that:

(1) There are distinctive temperature differences between different percentage prisms, and the temperature is higher for the higher fiber percentage prisms, though the difference between the 1.5% and 2.0% prisms is reversed at the beginning stage of heating;
(2) The temperature increments are reducing as the heating time increases;
(3) The temperature gaps between the 0.5% and 1.0%, the 1.0% and 1.5, and the 1.5% and 2.0% prisms become almost constant, increasing and saturating, respectively, as the heating time increases.

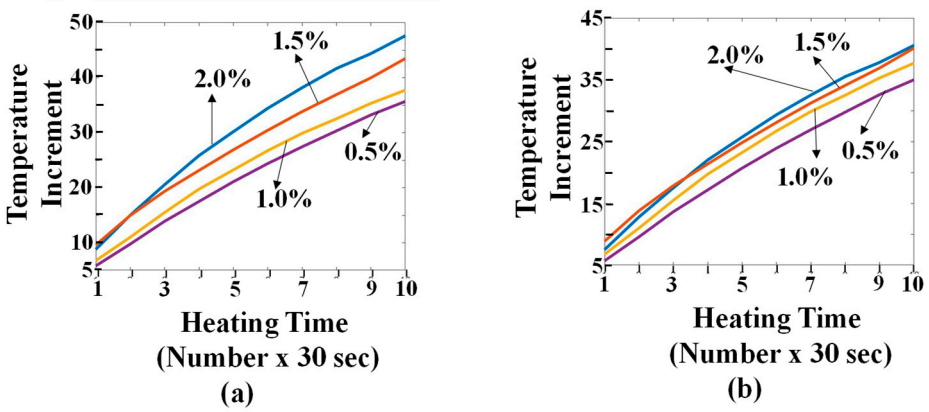

Figure 10. Comparisons of the surfaces' average temperature increments of four different percentage prisms: (**a**) Directly measured, (**b**) Compensated.

For Figure 10b, the temperature gap between 1.0% and 1.5% is slightly reduced, and between 1.5% and 2.0%, it almost disappears, but between 0.5% and 1.0%, it is increased. Due to this compensation, the temperature increments are slightly reduced for the 0.5% and 1.5% prisms, but they are significantly reduced for the 2.0% prism. Because of this reduction, the temperature difference between 1.5% and 2.0% almost disappears. In fact, the temperature of 2.0% (1.5%) at 5 min heating is reduced from 47.65° (43.5°) to 40.64° (40.19°). The difference between the two values is just 0.45°.

5. Conclusions

Electric current can flow through fiber-reinforced prisms due to the carbon fibers. Carbon fiber is a conductive material, and the amount of current flowing through the prisms depends on the voltage applied on them and the resistances introduced by the amount of fibers. When a constant power of 30 W is applied to each of the prisms reinforced by fibers of four different percentages, namely, 0.5%, 1.0%, 1.5% and 2.0%, the average temperature increment of the observed prism surface is greater for the higher percentage prisms. The heating efficiency of these prisms is higher for those of higher percentage, but the differences between them reduce as the heating time increases. The efficiency is in the range of 0.67 to 0.77 for the 5 min heating. The temperature increments for (1, 3) 5 min heating are (9.75°, 24.4°) 33.3°, (11.9°, 26.75°) 37.35°, (14.95°, 30.45°) 43.5° and (15.0°, 34.45°) 47.65° for the 0.5%, 1.0%, 1.5% and 2.0% prisms, respectively, as shown in Figure 10.

These values indicate that the highest increments are recorded at the first 1 min, and the increments are decreasing as the heating time length increases for all percentage prisms. The first 1 min also records the highest temperature increment for the lines representing the lowest and the highest temperature zones, and one of the normal lines to two electrodes, on the surfaces. In these cases, the increments at the first 1 min are higher than those for 1 to 3 min and 3 to 5 min heating. The physical reasons behind these facts are unclear as of now. The unchanging temperature ratio of two points on the surface during the 5 min heating also requires explanation.

Author Contributions: Conceptualization, J.-Y.S. and J.P.; methodology, J.-Y.S. and J.K.; software, J.K. and G.H.; validation, J.-Y.S. and T.V.; formal analysis, J.-Y.S., J.K. and G.H.; investigation, J.-Y.S., J.K., J.P. and G.H.; resources, J.K. and J.P.; data curation, J.K. and J.P.; writing—original draft preparation, J.-Y.S.; writing—review and editing, J.-Y.S. and T.V.; visualization, J.K.; supervision, G.H. and J.P.; project administration, G.H.; funding acquisition, G.H. and J.P. All authors have read and agreed to the published version of the manuscript.

Funding: Priority Reseach Centers Program through the National Reseach Foundation of Korea (NRF) funded by the Ministry of Education (Grant Number: NRF-2018R1A6A1A03025542).

Institutional Review Board Statement: Not applicable.

Informed Consent Statement: Not applicable.

Data Availability Statement: Not applicable.

Conflicts of Interest: The authors declare no conflict of interest.

References

1. Tabatabai, H.; Aljuboori, M. A Novel Concrete-Based Sensor for Detection of Ice and Water on Roads and Bridges. *Sensor* **2017**, *17*, 2912. [CrossRef] [PubMed]
2. Fay, L.; Clouser, K. Alternative Methods for Deicing, the Western Transportation Institute of Montana State University Bozeman, MT, Project 1003322/CR18-05 May 2020. Available online: https://clearroads.org/wp-content/uploads/dlm_uploads/FR_CR.18-05.pdf (accessed on 1 March 2023).
3. Jo, K.S.; Kim, N.I.; Kim, K.S.; Chu, Y.S.; Yoon, S.Y. A study on the electrical and physical properties of mortar incorporating carbon black. *JKCS* **2021**, *58*, 414–421. [CrossRef]
4. Sassani, A.; Arabzadeh, A.; Ceylan, H.; Kim, S.; Sadati, S.S.; Gopalakrishnan, K.; Taylor, P.C.; Abdualla, H. Carbon fiber-based electrically conductive concrete for salt-free deicing of pavements. *J. Clean. Prod.* **2018**, *203*, 799–809. [CrossRef]
5. Yehia, S.A.; Tuan, C.Y. Evaluation of Electrically Conductive Concrete Containing Carbon Products for Deicing. *ACI Mater. J.* **2004**, *101*, 287–293.
6. Zhao, H.; Wu, Z.; Wang, S.; Zheng, J.; Che, G. Concrete pavement deicing with carbon fiber heating wires. *Cold Reg. Sci. Technol.* **2011**, *65*, 413–420. [CrossRef]
7. Mohammed, A.; Ozgur, G.; Sevkat, E. Electrical resistance heating for deicing and snow melting applications: Experimental study. *Cold Reg. Sci. Technol.* **2019**, *160*, 128–138. [CrossRef]
8. Ahmet, B.K. Experimental Evaluation of Mechanical Properties and Fracture Behavior of Carbon Fiber Reinforced High Strength Concrete. *Period. Polytech. Civ. Eng.* **2016**, *60*, 289–296.
9. Han, B.; Zhang, L.; Zhang, C.; Wang, Y.; Yu, X.; Ou, J. Reinforcement effect and mechanism of carbon fibers to mechanical and electrically conductive properties of cement-based materials. *Constr. Build. Mater.* **2016**, *125*, 479–489. [CrossRef]
10. Benjamin, K.; Philipp, P.; Johann, K. Building lightweight structures with carbon-fiber-reinforced polymer-reinforced ultra-high-performance concrete: Research approach, construction materials, and conceptual design of three building components. *Struct. Concr.* **2018**, *20*, 730–744.
11. Zhang, Z.; Yang, W.; Cheng, L.; Cao, W.; Sain, M.; Tan, J.; Wang, A.; Jia, H. Carbon Fibers with High Electrical Conductivity: Laser Irradiation of Mesophase Pitch Filaments Obtains High Graphitization Degree. *ACS Sustain. Chem. Eng.* **2020**, *8*, 17629–17638. [CrossRef]
12. Morsy, R.; Marzouk, H.; Haddara, M.; Gu, X. Multi-channel random decrement smart sensing system for concrete bridge girders damage location identification. *Eng. Struct.* **2017**, *143*, 469–476. [CrossRef]
13. Badr, J.; Fargier, Y.; Palma-Lopes, S.; Deby, F.; Balayssac, J.; Delepine-Lesoille, S.; Cottineau, L.; Villain, G. Design and validation of a multi-electrode embedded sensor to monitor resistivity profiles over depth in concrete. *Constr. Build. Mater.* **2019**, *223*, 310–321. [CrossRef]
14. *KS L ISO 679*; Methods of Testing Cements-Determination of Strength. Korean Standards Association: Seoul, Republic of Korea, 2016; pp. 1–16.

15. Heo, G.; Kim, J.; Yim, C.; Tetiana, V.; Son, J.-Y. Carbon Fiber Traces in Cracked Surfaces of Mortar Prisms. *Appl. Sci.* **2022**, *12*, 2110. [CrossRef]
16. Park, J.; Heo, G.; Kim, J.; Venkel, T.; Son, J.Y. Detecting crack on-set time in mortar prisms with a thermal image. *Nondestruct. Test. Eval.* **2022**, *38*, 313–330. [CrossRef]
17. Electrically Conductive Adhesives. Available online: https://www.permabond.com/resource-center/electrically-conductive-adhesives (accessed on 1 March 2023).
18. Lataste, J.F. *Improvement of Electrical Resistivity Measurement for Nondestructive Assessment of Concrete Structures*, 2nd ed.; RILEM Publications SARL: Paris, France, 2003; pp. 5–6.
19. Houssam, A.T.; Tahar, E.-K.I.; Nathan, K.R. Strength and reliability of carbon-fiber-reinforced cement composites. *Cem. Concr. Compos.* **1994**, *16*, 15–21.
20. Kraus, J.D.; Carver, K.R. *Electromagnetics*; McGraw Hill: New York, NY, USA, 1973; pp. 109–112, ISBN 10: 0070853886.
21. Knight, R. *Physics for Scientists and Engineers*, 3rd ed.; Pearson: London, UK, 2013; p. 279.
22. Shafigh, P.; Asadi, T.; Akhiani, A.R.; Mahyuddin, N.B.; Hashemi, M. Thermal properties of cement mortar with different mix proportions. *Mater. De Constr.* **2020**, *70*, 9219. [CrossRef]
23. Fluke Handheld Multimeter. Available online: https://www.fluke.com/en-us/products/electrical-testing/digital-multimeters?query=fluke%2019 (accessed on 1 March 2023).